Nickel biosorption using Gracilaria caudata and Sargassum muticum

Yeslié González Bermúdez, Ivan Rico, Omar Gutiérrez Bermúdez, Guibal Eric

Nickel biosorption using *Gracilaria caudata* and *Sargassum muticum*

Yeslié González Bermúdez[a,b], Ivan L. Rodríguez Rico[a], Omar Gutiérrez Bermúdez[a], Eric Guibal[b,*]

[a] *Universidad Central de Las Villas, Department of Chemical Engineering, Camajuaní road, km 5 1/2, Santa Clara, Cuba*
[b] *Ecole des Mines d'Alès, Laboratoire Génie de l'Environnement Industriel, Equipe BPCI, 6 avenue de Clavières, F-30319 Alès Cedex, France*

A B S T R A C T

Two seaweeds (*Sargassum muticum*, *S.m.* and *Gracilaria caudata*, *G.c.*) collected on the coasts of Cuba have been tested and compared for nickel biosorption. The metal was efficiently bound to the biomass at pH 3 for *S.m.* and pH 5 for *G.c.* Sorption isotherms, at the optimum pH, showed that *S.m.* is more efficient than *G.c.*: maximum sorption capacity reached about 70 mg Ni g^{-1} and 45 mg Ni g^{-1} for *S.m.* and *G.c.*, respectively. The isotherms were modeled using the Langmuir equation (which fits better experimental data than the Freundlich and Temkin equations). Sorption kinetics were also carried out varying metal concentration, sorbent dosage particle size and temperature. The kinetics were modeled using the pseudo-second order rate equation and the intraparticle diffusion equation.

Keywords:
Biosorption
Algae
Nickel
Kinetics
Isotherms
Sargassum
Gracilaria

1. Introduction

The regulations concerning the discharge of contaminants to the environment are becoming more and more stringent. For example, metal ions may induce strong impact on the quality of water bodies, on wild and domestic life, and consequently on human health. Additionally, in many countries the discharge of a waste material in landfill is only authorized when the user has proved that the material cannot be valorized or recycled. These constraints have motivated a number of processes for recovering metals from effluents or waste materials. For example, recycling and metal recovery from spent batteries has retained a great attention in the research community for the last decade, based on the evolution of discharge regulations [1].

A number of processes exist for the treatment of metal-bearing solutions, including sorption on mineral sorbents [2], on ion exchange and chelating resins [3–5], on extractant impregnated resin [6,7], chemical precipitation [1,8], or membranes processes [9]. However, these processes frequently meet limiting criteria that make their application uncompetitive. Technical limitations (concentrations reached by the process), economical constraints (cost of the materials for large-size applications, energy consumption), environmental criteria (production of highly contaminated sludge or sorbent, poorly recyclable or difficultly valorizable) are some of the issues that may explain the need for alternative treatment processes. Biosorption has been widely investigated for the last decades, being considered a promising alternative to conventional processes [10]. Biosorption consists in using a biomass (produced from microorganisms, agriculture waste, biopolymers) for the binding of metal ions [11], dyes [12], organic compounds through a wide range of physico-chemical mechanisms, including ion exchange, chelation, complexation, precipitation. A great diversity of biosorbents has been carried out for metal binding. For example, bacterial cells [13,14], fungal biomass [15,16], algal biomass [17–23], stabilized anaerobic sludge [24,25], agriculture waste [26], crab shell [27–29], biopolymers [30–34] have been tested for nickel biosorption.

Algal material has a strong affinity for divalent cations. The binding efficiency is commonly explained by the presence of several polysaccharides in their cell walls: alginate [34–39] and fucoidan [40]. A numerous literature exists on metal interactions with alginate. It is commonly accepted that divalent metal cations interact with guluronic and mannuronic acids (the units constituting alginate biopolymer) through the "egg box" mechanism. Metal cations interact with carboxylic groups to form a dense network. Actually, this interaction can be also used for the ionotropic gelation of alginate to prepare hydrogels.

This study investigates the potential of two seaweeds, *Gracilaria caudata* and *Sargassum muticum*, endemic macroalgae from Cuban coasts (but also invasive in several countries over the world, including Europe) for biosorption. These biosorbents were tested for Ni(II) sorption. Nickel is known for having allergic effects (contact allergy through skin sensitivity causing dermatitis) at low concentration, while high-level exposure can induce lung and nasal sinus cancers

* Corresponding author. Tel.: +33 0466782734; fax: +33 0466782701.
E-mail address: Eric.Guibal@mines-ales.fr (E. Guibal).

depending on the administration mode (carcinogenesis effects). Nickel causes oxidative stress and may induce nausea, dizziness and diarrhea. EPA sets the admissible levels in drinking water to 0.04 mg L^{-1} [41]. The WHO guideline value was fixed to 0.07 mg L^{-1} [42].

The first part of the study checks the impact of pH on sorption performance (and acid–base/charge characteristics of the biosorbents). The sorption isotherms are established at the optimum pH and at different temperatures in order to evaluate the thermodynamics of the systems. The last part carries out the uptake kinetics varying sorbent dosage, sorbent particle size, temperature and metal concentration in order to evaluate the contribution of resistance to intraparticle diffusion on the control of sorption kinetics.

2. Materials and methods

2.1. Biomass

Two different algal biomass were tested: *Sargassum muticum* (*S.m.*), a brown algae collected on the north coast of Cuba (Caibarién beach), and *Gracilaria caudata* (*G.c.*), a red algae collected on the south coast of Cuba (close to Cienfuegos). After being collected, the biomass was repeatedly washed with demineralized water to remove impurities and cations such as Ca^{2+} and Na^{+}, dried in an oven (at 60 °C) and stored in desiccators. In order to investigate the impact of particle size, the biomass was grinded and sieved into three fractions: 125–250 μm, 250–500 μm and 710–1000 μm.

2.2. Characterization of biosorbents

The water content of the biosorbent was evaluated by weight loss at 60 °C overnight (higher temperature could induce a partial degradation of the biomass); the drying time was sufficient to reach constant weight.

The analysis of biosorbent charge was performed by titration using the method of pH derivation (pH of zero charge). The biomass (i.e., 50 mg) was added to a water solution (i.e., 100 mL), which pH was adjusted to target values (i.e., between pH 3 and 11) using 0.1 M solutions of HCl or NaOH. The suspension was maintained under agitation (at 150 rpm) for 48 h. The pH of zero charge (pH_{pzc}) was determined as the pH corresponding to the crossing of the curve $pH_{eq} = f(pH_i)$ with the first bisector ($pH_{eq} = pH_i$).

2.3. Sorption experiments

A stock solution of Ni(II) was prepared at the concentration of 1 g L^{-1} using $Ni(NO_3)\cdot 6H_2O$ in demineralized water (adding a drop of nitric acid to stabilize the solution). This stock solution was used for the preparation of test solutions by dilution (in the range 0–150 mg Ni L^{-1}, for sorption isotherms; at 10 mg Ni L^{-1} for investigating the pH effect); the pH was controlled to target value using 0.1 M solutions of HCl or NaOH. The biomass was added to the solution (sorbent dosage: 0.5 g L^{-1}) and the suspension was maintained under agitation (at the velocity of 150 rpm) on a reciprocal shaker for 48 h. The pH was not controlled during the sorption process but the equilibrium pH was systematically measured. Samples were collected and filtrated on a cellulose filter membrane (pore size: 1–2 μm). A drop of concentrated acid was systematically added to stabilize the filtrate and for analytical purpose. Metal concentration was determined by ICP-AES (inductively coupled plasma atomic emission spectrometry) using a Jobin Yvon Activa M (Jobin-Yvon, Longjumeau, France). Full experimental conditions (sorbent dosage, pH, metal concentration, temperature, etc.) are reported in the caption of the figures. The sorption capacity (q, mg Ni g^{-1}, or mmol Ni g^{-1}) in the biomass is determined by the mass balance equation: $q = (C_0 - C_{eq}) \times V/m$; where C_0 and C_{eq} are the initial and final concentrations of Ni(II) in the solution, V (L) is the volume of solution and m (g) is the sorbent amount. The sorption efficiency (SE: $100 \times (C_0 - C_{eq})/C_0$, %) was plotted versus equilibrium pH for pH optimization (SE versus pH_{eq}); while for sorption isotherms the sorption capacity was plotted versus equilibrium metal concentration in the solution (q versus C_{eq}).

For uptake kinetics, a given amount of sorbent was added to a pre-stabilized solution (target metal concentration and pH), samples were collected at fixed contact times, filtrated using a filter membrane, acidified and finally analyzed using ICP-AES. Unless specified (for target experiments) the sorbent dosage was set to 0.5 g L^{-1}, the temperature was fixed to 20 °C. The standard particle size was 125–250 μm, and the agitation speed was set at 150 rpm. The final pH was measured. The relative concentration ($C(t)/C_0$) was plotted versus time for comparing kinetic profiles.

2.4. Modeling of sorption isotherms and uptake kinetics

Sorption isotherms represent the distribution of the solute at equilibrium between the solid phase (the sorbent) and the liquid phase (the solution). The plot of q versus C_{eq} can be modeled using a number of equations. Though the equations of Freundlich and Langmuir are the most commonly used, alternative equations such as the Langmuir–Freundlich and the Temkin equations have also been cited [43].

$$\text{Langmuir}: \quad q = \frac{q_m b C_{eq}}{1 + b C_{eq}} \tag{1}$$

with q_m (mg Ni g^{-1} or mmol Ni g^{-1}), b (L mg^{-1} or L $mmol^{-1}$) are the constants of the Langmuir equation that were determined by a non-linear regression correlation method.

$$\text{Freundlich}: \quad q = k_F C_{eq}^{1/n} \tag{2}$$

with k_F ($mg^{1-1/n}\,L^{1/n}\,g^{-1}$ or $mmol^{1-1/n}\,L^{1/n}\,g^{-1}$) and n are the constants of the Freundlich equation.

$$\text{Temkin} \quad q = \frac{RT}{b_{Te}} \ln(a_{Te} C_f) \tag{3}$$

with a_{Te} (L g^{-1}) and b_{Te} (J mol^{-1}) are the constants of the Temkin equation.

$$\text{Langmuir–Freundlich}: \quad q = \frac{q_{m,LF} b_{LF} C_{eq}^{\alpha}}{1 + b_{LF} C_{eq}^{\alpha}} \tag{4}$$

with $q_{m,LF}$ (mg Ni g^{-1} or mmol Ni g^{-1}), b_{LF} ($(L\,mg^{-1})^{1/\alpha}$ or $(L\,mmol^{-1})^{1/\alpha}$) and α are the constants of the Langmuir–Freundlich equation.

The modeled curves frequently meet difficulties for correctly modeling the curved section of the isotherms. They overestimate sorption capacity in the intermediary section of the curve. Escudero et al. used a bi-site Langmuir equation for the modeling of hexanol using alginate aerogels [44]. This behavior is typical of systems involving several types of sorption sites with different adsorption energies. Assuming that several sites could be involved in the binding, the Langmuir equation becomes:

$$q = \frac{q_{m,1} b_1 C_{eq}}{1 + b_1 C_{eq}} + \frac{q_{m,2} b_2 C_{eq}}{1 + b_2 C_{eq}} \tag{5}$$

where ($q_{m,1}$,b_1) and ($q_{m,2}$,b_2) are the parameters for the two types of sorption sites.

The affinity coefficients (b_1 and b_2) may be significantly different reflecting the differences in strength of the interaction of the solute with these different sorption sites. The same concept can be applied to systems where the reactive groups interact with different metal species for which they have different affinities. This is especially

important when the metal speciation is strongly influenced by the composition of the solutions (hydrolysis, presence of ligands) [45].

The kinetics have been modeled using three conventional models: (i) the pseudo-first order rate equation (the so-called Lagergren equation), (b) the pseudo-second order rate equation [46], and (c) the simplified approach of intraparticle diffusion, the so-called Crank equation [47].

Pseudo-first order equation (PFORE) [48]:

$$\frac{dq(t)}{dt} = k_1(q_{eq} - q(t)) \tag{6a}$$

and after integration:

$$\ln\left(1 - \frac{q(t)}{q_{eq}}\right) = -k_1 t \tag{6b}$$

where q_{eq} (mg g^{-1}) is the sorption capacity at equilibrium (experimental value), k_1 (min^{-1}) is the pseudo-first order rate constant.

Pseudo-second order rate equation (PSORE) [46]:

$$\frac{dq(t)}{dt} = k_2(q_{eq} - q(t))^2 \tag{7a}$$

and after integration:

$$q(t) = \frac{q_{eq}^2 k_2 t}{1 + q_{eq} k_2 t} \tag{7b}$$

After linearization:

$$\frac{t}{q(t)} = \frac{1}{k_2 q_{eq}^2} + \frac{1}{q_{eq}} t \tag{7c}$$

where q_{eq} (mg g^{-1}) is the sorption capacity at equilibrium (calculated value from experimental data), k_2 (g mg^{-1} min^{-1}) is the pseudo-second order rate constant.

The intraparticle diffusion coefficient (D_{eff}, effective diffusivity, m^2 min^{-1}) has been determined using the Crank's equation, assuming the solid to be initially free of metal, external diffusion resistance not being limiting at long contact time [47]:

$$\frac{q(t)}{q_{eq}} = 1 - \frac{6}{\pi^2} \sum_{n=1}^{\infty} \frac{6\alpha(\alpha+1)\exp(-D_{eff} q_n^2 t / r^2)}{9 + 9\alpha + q_n^2 \alpha^2} \tag{8a}$$

q_n non-zero roots of the equation:

$$\tan q_n = \frac{3 q_n}{3 + \alpha q_n^2} \tag{8b}$$

with

$$\frac{q}{VC_0} = \frac{1}{1+\alpha} \tag{8c}$$

and r being the radius of the particle.

The parameters for the different models (for both isotherms and kinetics) were determined using the Mathematica® package (which also gives the estimated variance under selected format of experimental entries).

3. Results and discussion

3.1. Effect of pH on Ni(II) biosorption

3.1.1. Effect of pH on sorption efficiency

The pH of the solution is a key parameter for the evaluation of sorption performance. Its effect can be attributed to different causes: (a) impact on the reactive groups present at the surface of the sorbent (protonation/deprotonation effects), or (b) metal speciation [45,49]. In the case of Ni(II) sorption (in the absence of specific ligands in the solution) the speciation of the metal is not changed by the pH and the main effect will be explained by the impact of this parameter on the functional groups of the biomass.

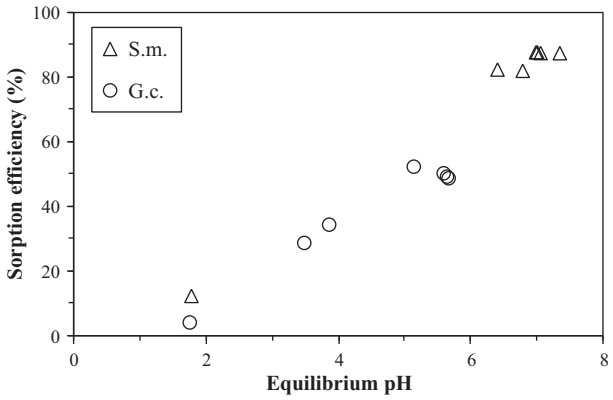

Fig. 1. Effect of pH on Ni(II) biosorption using *Sargassum muticum* and *Gracilaria caudata* (agitation speed: 150 rpm; agitation time: 48 h; *T*: 20 °C; particle size: 125–250 μm; sorbent dosage (SD): 0.5 g L^{-1}).

Fig. 1 compares the sorption efficiency for the two biosorbents for different initial pHs (ranging between 2 and 6). For both *S.m.* and *G.c.* the sorption efficiency increases with equilibrium pH. This general trend is consistent with the abundant literature on metal cation binding on biosorbents. This can be attributed to a decrease of the competition of protons for binding on reactive groups (also correlated to the progressive deprotonation of sorption sites such as carboxylic groups). Assuming that the most reactive groups are brought by alginate fraction in the biomass, the pK_a of carboxylic groups on the biomass are generally found between 2 and 4 [50,51]. However, substantial differences can be observed between the two biosorbents: while *G.c.* biomass maintains sorption efficiency below 50% with an equilibrium pH below 6, *S.m.* reaches sorption efficiency close to 90% under selected experimental conditions. In addition, it is possible to observe that the equilibrium pH for *S.m.* is substantially increased up to 7–7.3. At pH close to 7, the chemical conditions in the solution are close to the precipitation of Ni(II) based on the calculations of the MEDUSA software [52]. However, the simulation of the current experimental conditions with the Visual MINTEQ software makes debatable the occurrence of precipitation at pH 7–7.3 [53]. The differences in pH variation show that the characteristics of the biosorbents are substantially different.

3.2. Biosorbent titration

For these reasons a potentiometric-titration study was performed on the two biosorbents (Fig. 2) (note: these experiments were performed in nickel-free solutions). For *G.c.*, the pH remained approximately constant (varying by less than 0.2 pH unit) after metal sorption in the range pH 2–6; above, the biosorbent tends to stabilize the pH around a value in the range 6–6.7 (for pH$_i$ varying between 6 and 10). The intersection between the curve pH$_{eq}$ = *f*(pH$_i$) and the first bisector is close to pH 6. In the case of *S.m.*, the acid–base behavior of the sorbent is quite different with a significant pH increase: at pH$_i$ 4, the equilibrium pH approached pH 7 and maintained around pH 8 in the pH$_i$ range 6–10. The pH-stabilizing effect for *S.m.* is stronger (larger pH range) than for *G.c.*, and at a higher pH value (about two pH units). The pH increase was attributed to the dissolution of cytoplasmic compounds and ions present in the algal biomass [54].

Taking into account the acid–base properties of these materials and in order to prevent metal precipitation at high pH, the operating initial pH was selected to pH 3 for *S. muticum* and to pH 5 for *G. caudata*. With the increase of pH in the solution due to biosorption

Table 1
Modeling of Ni(II) sorption isotherms—comparison of isotherm equations (initial pH: 3 and 5 for *S. muticum* and *G. caudata*, respectively).

Model	Parameter	*S. muticum*	*G. caudata*
Langmuir	q_m (mg g^{-1})	75.6	50.1
	b (L mg^{-1})	0.0547	0.0455
	EV	14.8	8.7
Freundlich	k	12.76	7.83
	n	2.78	2.73
	EV	11.6	4.2
Temkin	a_{Te} (L g^{-1})	0.76	0.63
	b_{Te} (J mol^{-1})	163.9	245.5
	EV	12.1	6.1
Langmuir–Freundlich	q_m (mg g^{-1})	119.6	216.8
	b (L mg^{-1})	0.0799	0.0339
	α	0.592	0.427
	EV	10.1	4.5
Langmuir bi-site	$q_{m,1}$ (mg g^{-1})	69.4	59.5
	b_1 (L mg^{-1})	0.0615	0.0063
	$q_{m,2}$ (mg g^{-1})	10.0	20.0
	b_2 (L mg^{-1})	0.0077	0.291
	EV	16.3	4.5

EV: estimated variance.

addition the resulting charge of the biomass is negative making possible the binding of metal cations (proton exchange with metal cations). The equilibrium pH values remain consistent with metal solubility.

3.3. Sorption mechanism

FT-IR spectra were not collected in the present study; however, Sheng et al. investigated the sorption of *Sargassum* sp. and *Gracilaria* sp. for a series of metal cations (including Ni(II)) [21]. They observed the same increase of sorption capacity with pH. They characterized the biosorbents using XPS analysis and FT-IR spectroscopy. They correlated the enhancement of sorption with pH to the presence of weak carboxylic acid groups (R–COO$^-$) (apparent pK_a in the range 3.5–5.0) for alginate-rich algae; indeed, fucoidan bearing sulfonic acid groups (apparent pK_a in the range 1–2.5) poorly contributes to biosorption. The biomass containing hydroxyl groups may also adsorb at high pH due to their negative charge. They showed that FT-IR spectra were poorly changed after metal sorption in the wavenumber range representative of fucoidan (i.e., 1250 cm^{-1}) while the bands representative of carboxylate groups were significantly shifted (by 200 cm^{-1}) after metal binding (at ≈1630 cm^{-1} and ≈1420 cm^{-1}, for asymmetrical and symmetrical stretching bands, respectively). Some shifts were also observed

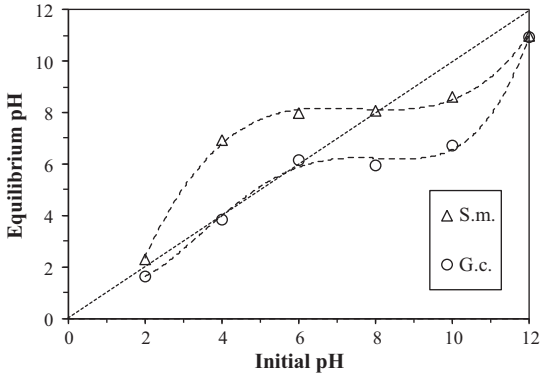

Fig. 2. Biomass (*S. muticum* and *G. caudata*) titration—equilibrium pH versus initial pH (continuous lines are not modeled curves; they just contribute to visualize the trends).

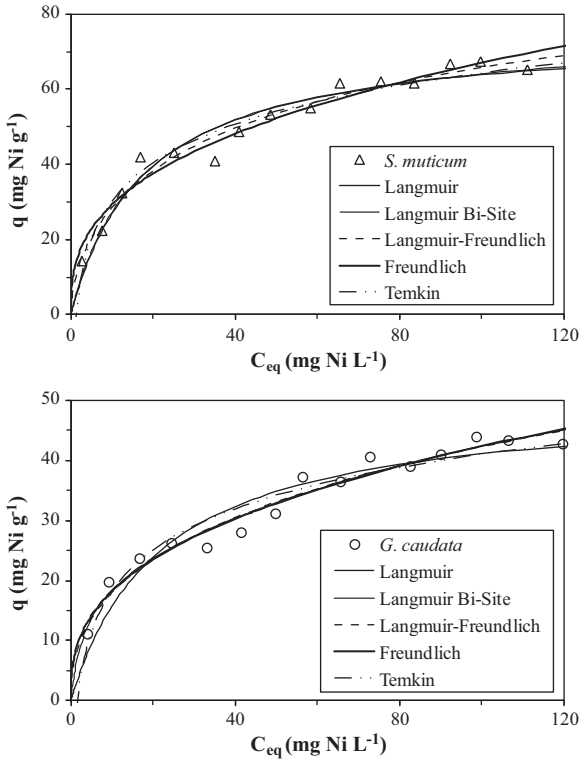

Fig. 3. Comparison of different models for the modeling of sorption isotherms for Ni(II) recovery using *S. muticum* (*S.m.*) and *G. caudata* (*G.c.*) (initial pH: 3 and 5 for *S. muticum* and *G. caudata*, respectively).

close to 1126 cm^{-1} and 1070 cm^{-1} (for –C–O stretching of ether groups, and –C–O stretching of alcoholic groups, respectively) and close to 1525 cm^{-1} for amine groups [21]. They suggest that most of metal sorption through chelation on carboxylic groups (bidentate complex) with contribution of alcoholic groups and amine groups to a lesser extent.

3.4. Sorption isotherms

3.4.1. Sorption isotherms at 20 °C modeling

In a first step, the sorption isotherms were performed at room temperature at the optimum pH value (Fig. 3). *S. muticum* reached a maximum sorption capacity close to 65 mg Ni g^{-1}, slightly higher than the level reached with *G. caudata* (i.e., 45 mg Ni g^{-1}) (Table 1). These values are consistent with those found in the literature concerning Ni(II) biosorption using algae (Table 2). The higher sorption capacities for *S.m.* than for *G.c.* may be explained by different com-

Table 2
Comparison of maximum Ni(II) sorption capacity for different algal biosorbents.

Biosorbent	pH_i	Sorption capacity (mg Ni g^{-1})	Reference
Chlorella vulgaris, free or immobilized	5	14–31	[17]
C. vulgaris	4.5	48–60	[56]
C. vulgaris immobilized	4–5	48–60	[57]
Sargassum sp. and *Padina* sp.	5.5	35	[21]
Ulva sp. and *Gracilaria* sp.	5.5	17	[21]
Laminaria japonica immobilized	4–7	40	[58]
Undaria pinnatifida	4.7	25	[18]
Enteromorpha prolifera	2–5	49–65	[59]
Sargassum wightii	4	20–26	[60]
Cystoseira indica	6	111–132	[61]
Sargassum muticum	5	70	This study
Gracilaria caudata	5	45	This study

Table 3
Influence of temperature on Ni(II) sorption isotherms using *S. muticum* and *G. caudata*—parameters of the Langmuir equation (initial pH: 3 and 5 for *S. muticum* and *G. caudata*, respectively).

Temperature (K)	*S. muticum*			*G. caudata*		
	q_m (mg Ni g^{-1})	b (L mg^{-1})	EV	q_m (mg Ni g^{-1})	b (L mg^{-1})	EV
293	75.6	0.055	14.8	50.1	0.046	8.7
303	59.0	0.038	37.1	–	–	–
323	41.5	0.031	6.1	41.7	0.030	16.9

positions of the cell wall of the algae, and more specifically different contents of alginate and even different guluronic/mannuronic acid ratio. Since the guluronic acid groups (G) are favorable to the formation of the "egg-box", contrary to mannuronic acid groups (M), high G/M molar ratios are favorable to the sorption of divalent cations [55]. Experimental data were modeled using Eqs. (2)–(6), and the parameters of these models are summarized in Table 1. All the models roughly fit experimental data (dots) with discrepancies that appear either in the initial section (low residual metal concentration) or in the curvature, or close to the saturation plateau. The EVs (estimated variance) of the different models are close enough to make difficult the selection of a model against the others, especially considering the different responses given by *S.m.* and *G.c.*; increasing the number of parameters in the model may contribute to improving the fitting of experimental data (loosing freedom degrees). However, the differences are not very marked. The EVs are systematically higher for *S.m.* than for *G.c.* The tendency of sorption capacity to stabilize above the residual concentration of 100 mg Ni L^{-1} (plateau) appears to be more consistent with equations that have asymptotic trend (contrary to Freundlich equations characterized by an exponential trend). In the concentration range tested in the study it was not possible identifying the saturation plateau and really discriminating between these models: it would be necessary increasing metal concentration. The affinity constant for the Langmuir constant (i.e., b coefficient) is close to 0.05 L mg^{-1} for both *S.m.* and *G.c.*, while the maximum sorption capacities are of the same order of magnitude (though slightly higher) than experimental maximum sorption capacities (i.e., 76 and 50 mg Ni g^{-1} versus 70 and 45 mg Ni g^{-1}, respectively). In the Freundlich model the coefficient n is also indicative of the affinity of the sorbent for the metal and the two biosorbents have a similar coefficient (close to 2.75 L mg^{-1}). The Langmuir–Freundlich and the Langmuir bi-site models gave very similar simulated plots of the sorption isotherms. For the Langmuir–Freundlich equation the maximum sorption capacities were much higher than the experimental maximum sorption capacity, the n coefficient was close to 0.5 (0.59 for *S.m.* and 0.43 for *G.c.*), while the affinity coefficient was more than doubled for *S.m.* compared to *G.c.* In the case of the Langmuir bi-site model, the values found for maximum sorption capacities $q_{m,1}$ and $q_{m,2}$ are consistent with experimental maximum sorption capacities for *S.m.* (i.e., 69 + 10 compared to 70 mg Ni g^{-1}) but much higher for *G.c.* (i.e., 60 + 20 compared to 45 mg Ni g^{-1}). While the affinity coefficients for the first reactive groups (i.e., b_1) are comparable for the two biosorbents, the other reactive groups are much higher for *G.c.* than for *S.m.* (0.29 L mg^{-1} versus 0.008 L mg^{-1}). The Temkin equation gave an intermediary simulated plot between the Langmuir plot and the other plots (Langmuir–Freundlich, Freundlich and Langmuir bi-site models). The coefficient b_{Te} varied around 0.7 J mol^{-1} for the two sorbents. These results confirm that *S. muticum* and *G. caudata* have comparable affinity for Ni(II) and that *S. muticum* has a higher sorption capacity than *G. caudata* probably due to a higher content of carboxylate groups (alginate). The differences in the modeling with the different equations are not very marked and the Langmuir equation will be used for the study of the effect of temperature.

3.4.2. Influence of temperature on sorption isotherms

Fig. 4 shows Ni(II) sorption isotherms at different temperatures (in the range 20–50 °C) for both *S. muticum* and *G. caudata*. The parameters of the Langmuir model are summarized in Table 3. Increasing the temperature induces a decrease in the sorption capacity for Ni(II), regardless of the biosorbent. However, the differences are more marked for *S.m.* than for *G.c.*: the sorption capacity was halved when increasing temperature from 20 °C to 50 °C for *S.m.*, while for *G.c.*, the same temperature increase diminishes sorption capacity by less 30%. The process is exothermic. This result contrasts with the biosorption of Ni(II) using *Chlorella vulgaris* [56]: in this case, the sorption capacity increased with temperature. The thermodynamic equilibrium constant K_c can be determined plotting q/C_{eq} versus C_{eq} and extrapolating this plot to 0 (not shown):

$$K_c = \lim_{C_{eq}\to 0}\left(\frac{q}{C_{eq}}\right) = q_m b \tag{9}$$

The thermodynamics can be described by the following equations:

$$\Delta G^0 = -RT\ln K_c \tag{10}$$

$$\ln K_c = \frac{\Delta s^0}{R} - \frac{\Delta H^0}{RT} \tag{11}$$

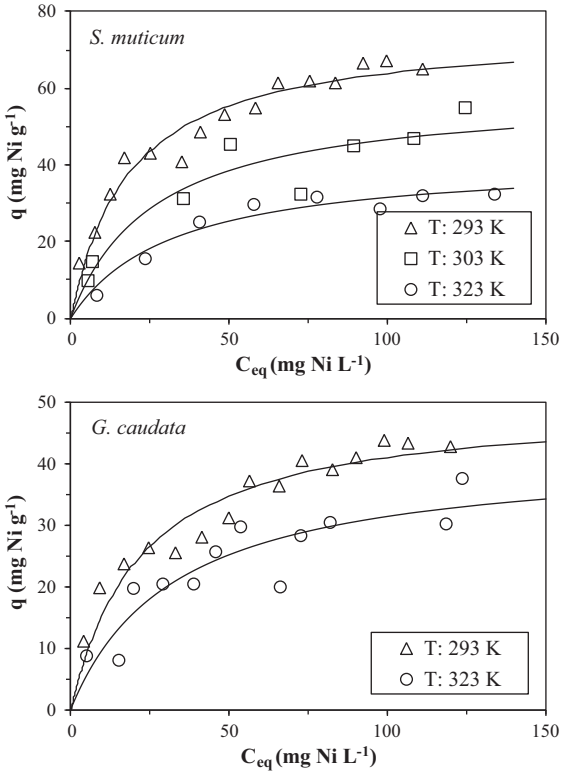

Fig. 4. Influence of temperature on Ni(II) sorption isotherms using *S. muticum* (*S.m.*) and *G. caudata* (*G.c.*) (initial pH: 3 and 5 for *S. muticum* and *G. caudata*, respectively).

with ΔG^0 is the Gibbs free energy of biosorption (kJ mol^{-1}), ΔH^0 is the enthalpy change of biosorption (kJ mol^{-1}) and ΔS^0 is the entropy change of biosorption (kJ mol^{-1} K^{-1}). Enthalpy change and entropy change are determined from the slope and intercept of the Van't Hoff plot ($\ln K_c$ versus $1/T$). Based on the limited number of temperatures investigated the values should only be considered as indicative of the order of magnitude of thermodynamic parameters. The standard enthalpy and entropy changes were −29.7 kJ mol^{-1} and −90.3 J mol^{-1} K^{-1} for *S. muticum* and −16.0 kJ mol^{-1} and −47.7 J mol^{-1} K^{-1} for *G. caudata*, respectively. The values of the thermodynamic parameters are roughly the double for *S.m.* compared to *G.c.*: this is consistent with the greater affinity of *Sargassum* biomass compared to *Gracilaria* material. The negative values of ΔH^0 are explained by the exothermic nature of the biosorption process. On the other hand, the negative values of ΔS^0 mean that during the biosorption the solid-solution interface reaches a more organized structure (decrease of randomness). For both *S. muticum* and *G caudata* the Gibbs free energy is negative; this means that the biosorption is spontaneous with high affinity for Ni(II). However, with increasing the temperature the absolute value of ΔG^0 decreases indicating that the affinity of the biosorbents diminishes. In the case of Ni(II) biosorption using *C. vulgaris* the mechanism was endothermic and the enthalpy change was significantly lower (about 11 kJ mol^{-1}) while the entropy change was greater (about 39 J mol^{-1} K^{-1}) [56].

3.5. Uptake kinetics

Four experimental parameters have been considered for their potential impact on uptake kinetics: sorbent dosage (SD), particle size (PS), initial metal concentration (C_0) and temperature (T). These parameters may influence external surface available for metal binding, diffusion properties (resistance to intraparticle diffusion, molecular diffusivity), and concentration gradient. The results are reported in Figs. 5–8 with superimposition of the curves simulated with the model of resistance to intraparticle diffusion (Eqs. (8a)–(8c)). The pseudo-first order and pseudo-second order rate equations were compared for modeling uptake kinetics and the PSORE model systematically gave a best fit of experimental curves (not shown). This is consistent with many studies that showed that the PSORE was more efficient for modeling kinetic profiles than the PFORE [62]. The modeling of experimental data with the PSORE is shown in section Additional Material (Figs. AM1–AM4). The parameters of the models are summarized in Table 4 (resistance to intraparticle diffusion) and Table 5 (PSORE): in most cases, the estimated variance was higher for the PSORE than for the resistance to intraparticle diffusion model. The specific surface area of this type of biomass is rather limited compared to conventional sorbents (mineral sorbents, synthetic resins), when they are not physically modified. For example, for *S. muticum* values like 11 m^2 g^{-1} were found; however, generally these values are limited to a few m^2 g^{-1} [63]. This is confirmed by the limited intraparticle porosity of these materials (below 9%) [63]. The sorption will mainly proceed at the surface of the biosorbent, limiting the contribution of internal reactive groups and then the effect of intraparticle diffusion mechanism.

3.6. Influence of sorbent dosage

The variation of sorbent dosage contributes to increasing the number of reactive groups (and thus the equilibrium performance) but also the surface in contact with the solution. This may impact the resistance to film diffusion. The model of resistance to intraparticle diffusion fits well experimental data. The intraparticle diffusion coefficient (D_{eff}) varies in the range

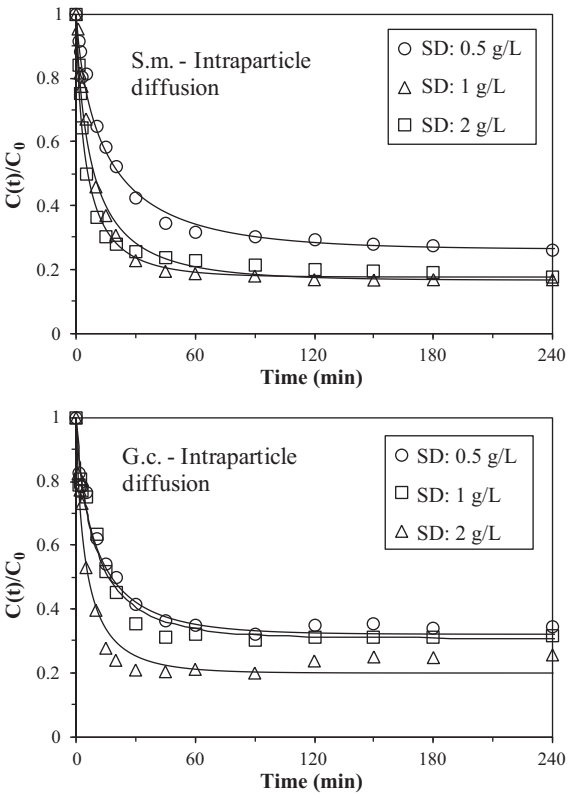

Fig. 5. Influence of sorbent dosage (SD) on Ni(II) uptake kinetics using *S. muticum* (*S.m.*) and *G. caudata* (*G.c.*)—modeling using the intraparticle diffusion coefficient (initial pH: 3 and 5 for *S. muticum* and *G. caudata*, respectively; *T*: 20 °C; *v*: 150 rpm; PS: 125–250 μm; C_0: 10 mg Ni L^{-1}).

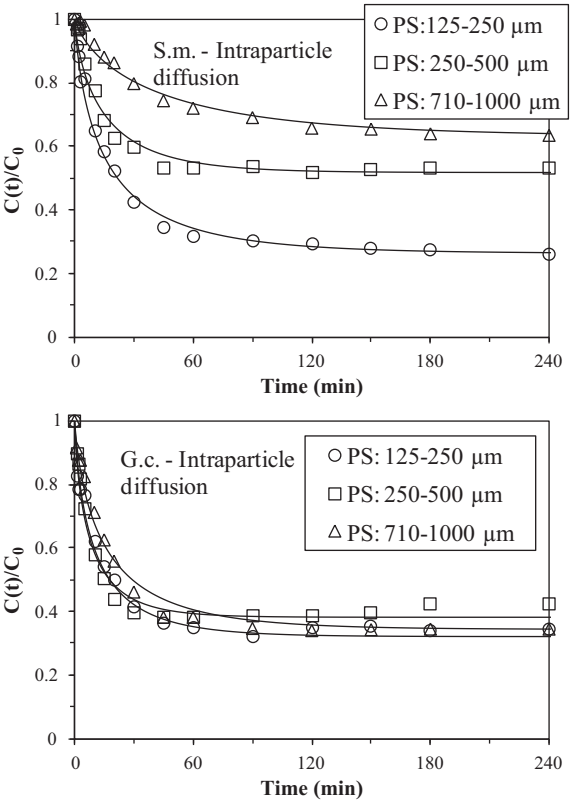

Fig. 6. Influence of particle size (PS) on Ni(II) uptake kinetics using *S. muticum* (*S.m.*) and *G. caudata* (*G.c.*)—modeling using the intraparticle diffusion coefficient (initial pH: 3 and 5 for *S. muticum* and *G. caudata*, respectively; *T*: 20 °C; *v*: 150 rpm; C_0: 10 mg Ni L^{-1}; SD: 0.5 g L^{-1}).

Table 4
Ni(II) uptake kinetics—parameters of the model of resistance to the intraparticle diffusion (Crank's equation).

Biosorbent	T	PS	SD	C_0	$D_{eff} \times 10^{11}$	EV
	293	125–250	0.5	10	3.8	0.012
	293	125–250	0.5	30	21.1	0.007
	293	125–250	0.5	50	9.4	0.040
	293	125–250	1	10	4.6	0.031
S. muticum	293	125–250	2	10	7.5	0.015
	303	125–250	0.5	10	5.9	0.047
	323	125–250	0.5	10	10.9	0.130
	293	250–500	0.5	10	29.4	0.057
	293	710–1000	0.5	10	64.5	0.048
	293	125–250	0.5	10	6.9	0.034
	293	125–250	0.5	30	4.9	0.015
	293	125–250	0.5	50	89.5	0.032
	293	125–250	1	10	7.1	0.047
G. caudata	293	125–250	2	10	8.6	0.048
	303	125–250	0.5	10	6.3	0.018
	323	125–250	0.5	10	19.2	0.152
	293	250–500	0.5	10	42.3	0.034
	293	710–1000	0.5	10	101.0	0.023

T (K); PS (μm); SD ($g\,L^{-1}$); C_0 ($mg\,Ni\,L^{-1}$); D_{eff} ($m^2\,min^{-1}$).

$(3.8–7.5) \times 10^{-11}\ m^2\,min^{-1}$ and $(6.9–8.6) \times 10^{-11}\ m^2\,min^{-1}$ for *S. muticum* and *G. caudata*, respectively. These values are 3 orders of magnitude lower than the values of the molecular diffusivity of Ni(II) in water (i.e., $3.97 \times 10^{-8}\ m^2\,min^{-1}$) [64]. This means that the diffusion of metal ions through the layers of the biosorbent is significantly hindered by the poor porosity of the material. The effective diffusivity is not expected to vary with sorbent dosage. Though D_e increases with SD, the values remain in the same order of magnitude and the differences between the two sorbents are not very marked. The slight variation may be caused by the occurrence of complementary limitations such as resistance to film diffusion or the proper reaction rate. It is generally necessary to simultaneously take into account all these mechanisms [43], at the expense of complex numerical calculations. Additionally, these complex numerical models require simplifying approximations (homogeneous material, spherical particles, and single reactive groups) that are generally far from the true properties and characteristics of materials such as biosorbents. For this reason the simplified Crank's equation will be considered acceptable, despite the small discrepancies due to variation of D_{eff} with SD. Table 5 shows that the kinetic rate (i.e., k_2) increases with SD with almost the same amplitude for the two sorbents (in the range $(0.5–6.7) \times 10^{-2}\ g\,mg^{-1}\,min^{-1}$). As expected, increasing SD decreases the sorption capacity and the sorption capacity obtained by the simulation is close to the experimental value.

3.7. Influence of particle size

Varying the particle size is generally used for evaluating the accessibility and the availability of reactive groups. If the equilibrium concentration is independent of the particle size, this means that all the reactive groups are accessible to solute molecules. On the opposite hand if the equilibrium concentration depends on sorbent particle size the solute cannot interact with internal reactive groups. Fig. 6 shows that *S. muticum* and *G. caudata* obey quite different behavior. With *G.c.* biomass the uptake kinetics were not affected by the size of sorbent particles: Ni(II) can bound on all reactive groups (even at the center of large particles; i.e., 710–1000 μm fraction). On the contrary, with *S.m.* very different kinetic profiles were observed when increasing the size of sorbent particles. The equilibrium concentration but also the time required to reach the equilibrium increase with the diameter of the particles. The superimposition of the kinetic profiles for *G.c.* indicates that this biomass is not subject to strong resistance to intraparticle diffusion. Table 4 shows that for both *S.m.* and *G.c.* the effective diffusivity linearly increased with the average of particle radius. The diffu-

Table 5
Ni(II) uptake kinetics—parameters of the pseudo-second order rate equation (PSORE).

Biosorbent	T	PS	SD	C_0	$q_{eq,exp}$	$q_{eq,mod}$	$k_2 \times 10^2$	EV
	293	125–250	0.5	10	14.5	15.4	0.54	0.21
	293	125–250	0.5	30	21.7	23.1	1.17	0.52
	293	125–250	0.5	50	47.8	50.1	0.32	3.76
	293	125–250	1	10	7.9	8.5	1.64	0.10
S. muticum	293	125–250	2	10	4.0	4.0	6.69	0.01
	303	125–250	0.5	10	12.1	13.5	0.85	0.74
	323	125–250	0.5	10	9.9	11.0	1.08	0.91
	293	250–500	0.5	10	11.5	12.6	0.69	0.54
	293	710–1000	0.5	10	7.4	9.0	0.28	0.09
	293	125–250	0.5	10	12.9	13.6	1.08	0.55
	293	125–250	0.5	30	19.2	19.4	3.11	0.56
	293	125–250	0.5	50	20.4	20.2	5.77	0.46
	293	125–250	1	10	6.7	7.2	2.00	0.21
G. caudata	293	125–250	2	10	3.5	3.9	6.59	0.06
	303	125–250	0.5	10	11.8	12.5	0.83	0.13
	323	125–250	0.5	10	11.5	13.2	3.07	1.95
	293	250–500	0.5	10	12.7	13.4	1.35	0.61
	293	710–1000	0.5	10	13.5	14.9	0.53	0.31

T (K); PS (μm); SD ($g\,L^{-1}$); C_0 ($mg\,Ni\,L^{-1}$); $q_{eq,exp}$ and $q_{eq,mod}$ ($mg\,Ni\,g^{-1}$); k_2 ($g\,mg^{-1}\,min^{-1}$).

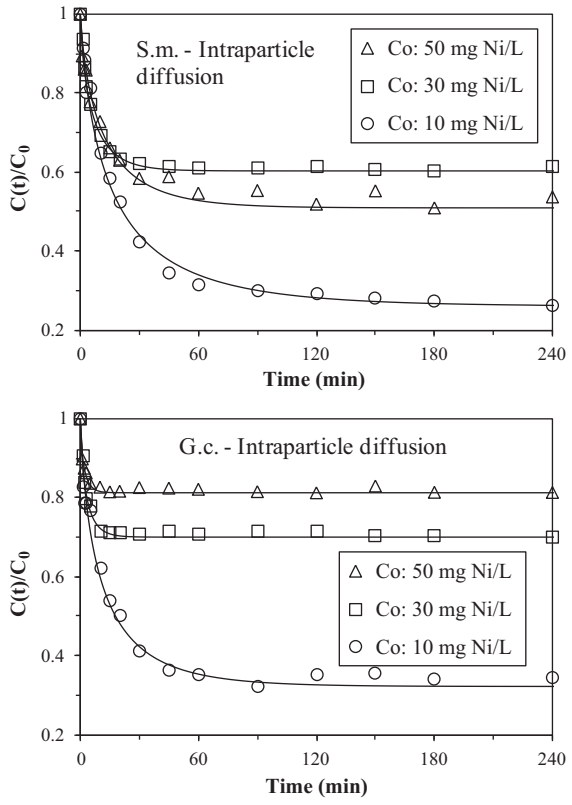

Fig. 7. Influence of metal concentration (C_0) on Ni(II) uptake kinetics using *S. muticum* (*S.m.*) and *G. caudata* (*G.c.*)—modeling using the intraparticle diffusion coefficient (initial pH: 3 and 5 for *S. muticum* and *G. caudata*, respectively; *T*: 20 °C; *v*: 150 rpm; PS: 125–250 μm; SD: 0.5 g L^{-1}).

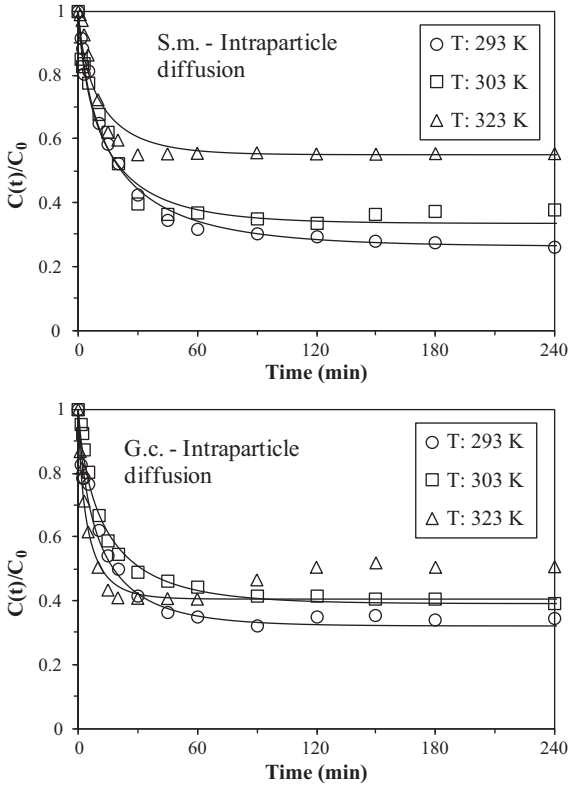

Fig. 8. Influence of temperature (*T*) on Ni(II) uptake kinetics using *S. muticum* (*S.m.*) and *G. caudata* (*G.c.*)—modeling using the intraparticle diffusion coefficient (initial pH: 3 and 5 for *S. muticum* and *G. caudata*, respectively; *v*: 150 rpm; C_0: 10 mg Ni L^{-1}, PS: 125–250 μm; SD: 0.5 g L^{-1}).

sion coefficient varies in the range $(3.8–65) \times 10^{-11}$ m^2 min^{-1} and $(6.9–101) \times 10^{-11}$ m^2 min^{-1} for *S. muticum* and *G. caudata*, respectively.

The particle size does not affect the sorption capacity at equilibrium for *G. caudata* while increasing the particle size reduces the sorption capacity for *S. muticum* for both experimental and modeled values (which are of the same order of magnitude): this is another evidence of the significant difference in the behavior of the two biosorbents. The difference in sorption capacity at equilibrium means that all the reactive groups in the inner part of sorbent particles are not accessible for *S.m.*. The kinetic rate constant k_2 does not follow a regular trend when increasing the size of sorbent particles. It varies between 0.28×10^{-2} and 0.69×10^{-2} g mg^{-1} min^{-1} for *S.m.* and between 0.53×10^{-2} and 1.35×10^{-2} g mg^{-1} min^{-1} for *G.c.*: the kinetic rate is about two times higher for *G.c.* (compared to *S.m.*).

3.8. Influence of metal concentration

Fig. 7 shows the impact of initial metal concentration on Ni(II) kinetic profiles (with the model of resistance to intraparticle diffusion) for both *S.m.* and *G.c.*; Tables 4 and 5 summarize the parameters of the models (PSORE and intraparticle diffusion resistance). Increasing metal concentration increases the concentration gradient between the solution and the center (free of metal) of the particles. This increase in gradient concentration enhances the transfer of the solute and reduces the time required to reach equilibrium. Some discrepancies were obtained in the experimental series especially for *S.m.*, where the equilibrium concentration was higher at C_0: 30 mg Ni L^{-1} than the value reached at C_0: 50 mg Ni L^{-1}, inducing, in turn, discrepancies in the trends of intraparticle diffusivities. The coefficient D_{eff} varies between 3.8×10^{-11} and 2.1×10^{-10} m^2 min^{-1} for *S.m.* while for *G.c.* the intraparticle diffusivity increased from 4.9×10^{-11} and 9.0×10^{-10} m^2 min^{-1}.

In the case of the PSORE, the sorption capacity at equilibrium calculated for the model is close to the experimental value (the differences do not exceed 10%) and logically increases with metal concentration. While for *G.c.* the kinetic rate coefficient follows a continuously increasing trend (from 1.1×10^{-2} to 5.8×10^{-2} g mg^{-1} min^{-1}), in the case of *S.m.* the variation of the parameter k_2 was discontinuous and less marked (in the range $(0.3–1.2) \times 10^{-2}$ g mg^{-1} min^{-1}).

3.9. Influence of temperature

The study of temperature effect on sorption isotherms has shown that this parameter has a greater impact on the sorption of Ni(II) using *S.m.* than with *G.c.*; this is confirmed by the comparison of uptake kinetics at different temperatures. In the case of *G.c.*, the kinetic profiles are quite close, though the intraparticle diffusivity increased from $(6.3–6.9) \times 10^{-11}$ m^2 min^{-1} to 19.2×10^{-11} m^2 min^{-1} when temperature increases from 20–30 °C to 50 °C. For *S.m.* the intraparticle diffusivity progressively and continuously increases with temperature (from 3.8×10^{-11} to 10.9×10^{-11} m^2 min^{-1}). Similar trends were observed with the PSORE kinetic rate: the coefficient k_2 increases with temperature for *S.m.*, and more discontinuously for *G.c.*. The Arrhenius plot of $\ln k_2$ versus the reciprocal of temperature allows determining the activation energy of the system (E_a, kJ mol^{-1}):

$$\ln k_2 = \ln A - \frac{E_a}{RT} \tag{12}$$

The slope of the curve (not shown) gives the activation energy. Since the kinetics were performed at only three different temperatures (with some little discrepancies) the values should be only considered as indicative of the order of magnitude. For *S.*

muticum, E_a is close to 30.5 kJ mol^{-1}, about almost two times the value obtained with G. *caudata* (i.e., 17.2 kJ mol^{-1}). Ayoob et al. correlated the activation energy in to the sorption mechanism: (a) 8–25 kJ mol^{-1} physical adsorption; (b) <21 kJ mol^{-1} to water diffusion; (c) 20–40 kJ mol^{-1} to pore diffusion; (d) >40 kJ mol^{-1} to ion exchange mechanism [65]. The greater contribution of the resistance to intraparticle diffusion on the kinetic control may explain the higher energy of activation found for *S.m.*.

4. Conclusion

Nickel ions can be efficiently sorbed on *Sargassum muticum* and *Gracilaria caudata* seaweeds, at initial pH 3 and 5, respectively. Sorption capacities are slightly higher for *S. muticum* than for *G. caudata*. Simultaneously to metal sorption the pH of the solution is significantly increased for *S. muticum* (the variation is much lower for *G. caudata*), consistently with the acid–base properties of the biosorbents. The sorption isotherms can be described by conventional Langmuir and Freundlich equations, though more sophisticated models (Temkin, Langmuir–Freundlich, or Langmuir bi-site equations) also gave good fits of experimental data. The sorption process is exothermic (negative value of the enthalpy): the sorption capacity decreases with increasing the temperature, especially for *S. muticum* biomass. Uptake kinetics have been modeled using both the model of resistance to intraparticle diffusion and the pseudo-second order rate equation. These two models gave comparable fits for experimental data. The sorbent dosage has a limited impact on uptake kinetics compared to metal concentration. When changing the size of sorbent particles significant differences were observed between *S. muticum* and *G. caudata*: while this parameter hardly affects sorption kinetics for *Gracilaria* biosorbent, with *S. muticum* the differences are more marked. This means that the resistance to intraparticle diffusion is playing an important role in the control of sorption kinetics (especially for *S.m.*). This is probably due to restricted accessibility to the reactive groups located at the center of the particles. The temperature had a limited effect on Ni(II) sorption kinetics on *G. caudata*, compared to *S. muticum*. The intraparticle diffusivity varied between 3.8×10^{-11} and 65×10^{-11} m^2 min^{-1} for *S. muticum* and between 4.9×10^{-11} and 101×10^{-11} m^2 min^{-1} for *G. caudata*. The activation energy that was roughly evaluated confirms that the sorption mechanism took place through physical sorption with contribution of resistance to intraparticle diffusion (especially for *S. muticum*).

Acknowledgement

Authors thanks European Union for financial support under the ALFA program (Contract AML/190901/06/18414/II-0548-FC-FA).

Appendix A. Supplementary data

Supplementary data associated with this article can be found, in the online version, at doi:10.1016/j.cej.2010.10.038.

References

[1] J.H. Li, X.H. Li, Q.Y. Hu, Z.X. Wang, J.C. Zheng, L. Wu, L.X. Zhang, Study of extraction and purification of Ni, Co and Mn from spent battery material, Hydrometallurgy 99 (2009) 7–12.

[2] Y.C. Sharma, V. Srivastava, S.N. Upadhyay, C.H. Weng, Alumina nanoparticles for the removal of Ni(II) from aqueous solutions, Ind. Eng. Chem. Res. 47 (2008) 8095–8100.

[3] V. Tharanitharan, K. Srinivasan, Removal of Ni(II) from water and wastewater using modified Duolite XAD-761 resin, Indian J. Chem. Technol. 16 (2009) 245–253.

[4] C. Duran, H.B. Senturk, L. Elci, M. Soylak, M. Tufekci, Simultaneous preconcentration of Co(II), Ni(II), Cu(II), and Cd(II) from environmental samples on Amberlite XAD-2000 column and determination by FAAS, J. Hazard. Mater. 162 (2009) 292–299.

[5] N. Dizge, B. Keskinler, H. Barlas, Sorption of Ni(II) ions from aqueous solution by Lewatit cation-exchange resin, J. Hazard. Mater. 167 (2009) 915–926.

[6] A.F. Ngomsik, A. Bee, J.M. Siaugue, V. Cabuil, G. Cote, Nickel adsorption by magnetic alginate microcapsules containing an extractant, Water Res. 40 (2006) 1848–1856.

[7] E. Guibal, T. Vincent, C. Jouannin, Immobilization of extractants in biopolymer capsules for the synthesis of new resins: a focus on the encapsulation of tetraalkyl phosphonium ionic liquids, J. Mater. Chem. 19 (2009) 8515–8527.

[8] J.M. Skowronski, M. Osinska, The determination of chemical precipitation conditions of nickel hydroxide from solutions after leaching spent Ni–Cd batteries, Przem. Chem. 88 (2009) 826–828.

[9] E.P. Kuncoro, J. Roussy, E. Guibal, Mercury recovery by polymer-enhanced ultrafiltration: comparison of chitosan and poly(ethylenimine) used as macroligand, Sep. Sci. Technol. 40 (2005) 659–684.

[10] N. Barka, M. Abdennouri, A. Boussaoud, M. El Makhfouk, Biosorption characteristics of cadmium(II) onto *Scolymus hispanicus* L. as low-cost natural biosorbent, Desalination 258 (2010) 66–71.

[11] N. Ertugay, Y.K. Bayhan, The removal of copper(II) ion by using mushroom biomass (*Agaricus bisporus*) and kinetic modelling, Desalination 255 (2010) 137–142.

[12] I. Kiran, S. Ilhan, N. Caner, C.F. Iscen, Z. Yildiz, Biosorption properties of dried Neurospora crassa for the removal of Burazol Blue ED dye, Desalination 249 (2009) 273–278.

[13] A. Lopez, N. Lazaro, S. Morales, A.M. Marques, Nickel biosorption by free and immobilized cells of *Pseudomonas fluorescens 4F39*: a comparative study, Water Air Soil Pollut. 135 (2002) 157–172.

[14] D. Gialamouidis, M. Mitrakas, M. Liakopoulou-Kyriakides, Biosorption of nickel ions from aqueous solutions by *Pseudomonas sp.* and *Staphylococcus xylosus* cells, Desalination 248 (2009) 907–914.

[15] Y. Sag, T. Kutsal, Copper (II) and nickel(II) adsorption by *Rhizopus-arrhizus* in batch stirred reactors in series, Chem. Eng. J. 58 (1995) 265–273.

[16] A. Tahir, S. Zahid, Ni(II) biosorption by Rhizopus arrhizus Env 3: the study of important parameters in biomass biosorption, J. Chem. Technol. Biotechnol. 83 (2008) 1633–1638.

[17] F.A. Abu Al-Rub, M.H. El-Naas, F. Benyahia, I. Ashour, Biosorption of nickel on blank alginate beads, free and immobilized algal cells, Process Biochem. 39 (2004) 1767–1773.

[18] Z Chen, W. Ma, M. Han, Biosorption of nickel and copper onto treated alga (*Undaria pinnatifida*): application of isotherm and kinetic models, J. Hazard. Mater. 155 (2008) 327–333.

[19] A. Esmaeili, S. Soufi, A. Rustaiyan, S. Safaiyan, S. Mirian, G. Fallahe, N. Moazami, Biosorption of copper, cobalt and nickel by marine brown alga *Sargassum sp.* in fixed-bed column, Pak. J. Biol. Sci. 10 (2007) 3919–3922.

[20] H.H. Omar, Biosorption of copper, nickel and manganese using non-living biomass of marine alga, *Ulva lactuca*, Pak. J. Biol. Sci. 11 (2008) 964–973.

[21] P.X. Sheng, Y.P. Ting, J.P. Chen, L. Hong, Sorption of lead, copper, cadmium, zinc, and nickel by marine algal biomass: characterization of biosorptive capacity and investigation of mechanisms, J. Colloid Interface Sci. 275 (2004) 131–141.

[22] K. Vijayaraghavan, J. Jegan, K. Palanivelu, A. Velan, Biosorption of copper, cobalt and nickel by marine green alga *Ulva reticulata* in a packed column, Chemosphere 60 (2005) 419–426.

[23] M. Reategui, H. Maldonado, M. Ly, E. Guibal, Mercury(II) biosorption using *Lessonia* sp. kelp Appl. Biochem. Biotechnol., in press.

[24] A.H. Hawari, C.N. Mulligan, Biosorption of lead(II), cadmium(II), copper(II) and nickel(II) by anaerobic granular biomass, Bioresour. Technol. 97 (2006) 692–700.

[25] A.H. Hawari, C.N. Mulligan, Effect of the presence of lead on the biosorption of copper, cadmium and nickel by anaerobic biomass, Process Biochem. 42 (2007) 1546–1552.

[26] K.S Baig, H.D. Doan, J. Wu, Multicomponent isotherms for biosorption of Ni^{2+} and Zn^{2+}, Desalination 249 (2009) 429–439.

[27] V.W.D. Chui, K.W. Mok, C.Y. Ng, B.P. Luong, K.K. Ma, Removal and recovery of copper(II), chromium(III), and nickel(II) from solutions using crude shrimp chitin packed in small columns, Environ. Int. 22 (1996) 463–468.

[28] S. Pradhan, S.S. Shukla, K.L. Dorris, Removal of nickel from aqueous solutions using crab shells, J. Hazard. Mater. 125 (2005) 201–204.

[29] K. Vijayaraghavan, J. Jegan, K. Palanivelu, M. Velan, Removal of nickel(II) ions from aqueous solution using crab shell particles in a packed bed up-flow column, J. Hazard. Mater. 113 (2004) 225–232.

[30] V.M. Boddu, K. Abburi, A.J. Randolph, E.D. Smith, Removal of copper(II) and nickel(II) ions from aqueous solutions by a composite chitosan biosorbent, Sep. Sci. Technol. 43 (2008) 1365–1381.

[31] S.R. Popuri, Y. Vijaya, V.M. Boddu, K. Abburi, Adsorptive removal of copper and nickel ions from water using chitosan coated PVC beads, Bioresour. Technol. 100 (2009) 194–199.

[32] B. Tanja, M. Schlaak, H. Strasdeit, Adsorption of nickel(II), zinc(II) and cadmium(II) by new chitosan derivatives, React. Funct. Polym. 44 (2000) 289–298.

[33] M. Zamin, T. Shaheen, M. Ahmed, Removal of nickel-63 ions from aqueous solutions by chitosan flakes, Ads. Sci. Technol. 22 (2004) 849–858.

[34] Y. Vijaya, S.R. Popuri, V.M. Boddu, A. Krishnaiah, Modified chitosan and calcium alginate biopolymer sorbents for removal of nickel(II) through adsorption, Carbohydr. Polym. 72 (2008) 261–271.

[35] E. Fourest, B. Volesky, Alginate properties and heavy metal biosorption by marine algae, Appl. Biochem. Biotechnol. 67 (1997) 215–226.

[36] Y. Kaçar, C. Arpa, S. Tan, A. Denizli, O. Genç, Y. Arica, Biosorption of Hg(II) and Cd(II) from aqueous solutions: comparison of biosorptive capacity of alginate and immobilized live and heat inactivated *Phanerochaete chrysosporium*, Process Biochem. 37 (2002) 601–610.
[37] J.P. Ibáñez, Y. Umetsu, Potential of protonated alginate beads for heavy metals uptake, Hydrometallurgy 64 (2002) 89–99.
[38] G. Bayramoglu, M.Y. Arica, Construction a hybrid biosorbent using *Scenedesmus quadricauda* and Ca-alginate for biosorption of Cu(II) Zn(II) and Ni(II): kinetics and equilibrium studies, Bioresour. Technol. 100 (2009) 186–193.
[39] R. Lagoa, J.R. Rodrigues, Evaluation of dry protonated calcium alginate beads for biosorption applications and studies of lead uptake, Appl. Biochem. Biotechnol. 143 (2007) 115–128.
[40] T.A. Davis, B. Volesky, A. Mucci, A review of the biochemistry of heavy metal biosorption by brown algae, Water Res. 37 (2003) 4311–4330.
[41] ATSDR, Toxicological Profiles, Agency for Toxic Substances and Disease Registry, U.S. Department of Health and Human Services, Public Health Service, Atlanta, GA, USA, 1999.
[42] WHO, Nickel in Drinking-water. Background Document for Development of WHO Guidelines for Drinking-water Quality, World Health Organization, Geneva, Switzerland, 2005.
[43] C. Tien, Adsorption Calculations Modeling, Butterworth-Heinemann, Newton, MA, 1994.
[44] R.R. Escudero, M. Robitzer, F. Di Renzo, F. Quignard, Alginate aerogels as adsorbents of polar molecules from liquid hydrocarbons: hexanol as probe molecule, Carbohydr. Polym. 75 (2009) 52–57.
[45] J. Guzman, I. Saucedo, J. Revilla, R. Navarro, E. Guibal, Copper sorption by chitosan in the presence of citrate ions: influence of metal speciation on sorption mechanism and uptake capacities, Int. J. Biol. Macromol. 33 (2003) 57–65.
[46] Y.S. Ho, Second-order kinetic model for the sorption of cadmium onto tree fern: a comparison of linear and non-linear methods, Water Res. 40 (2006) 119–125.
[47] J. Crank, The Mathematics of Diffusion, 2nd ed., Oxford University Press, Oxford, G.B., 1975.
[48] Y. Liu, Y.-Y. Liu, Biosorption isotherms, kinetics and thermodynamics, Sep. Purif. Technol. 61 (2007) 229–242.
[49] P. Chassary, T. Vincent, E. Guibal, Metal anion sorption on chitosan and derivative materials: a strategy for polymer modification and optimum use, React. Funct. Polym. 60 (2004) 137–149.
[50] A. Haug, O. Smidrod, Selectivty of some anionic polymers for divalent metal ions, Acta Chem. Scand. 24 (1970) 843–854.
[51] C. Rey-Castro, R. Herrero, M.E.S. de Vicente, Gibbs-Donnan and specific-ion interaction theory descriptions of the effect of ionic strength on proton dissociation of alginic acid, J. Electroanal. Chem. 564 (2004) 223–230.
[52] I. Puigdomenech, MEDUSA (Make equilibrium diagrams using sophisticated algorithms), v. 3.1, Royal Institute of Technology, Stockholm, Sweden, 2002.
[53] J.P. Gustafsson, Visual MINTEQ, KTH, Dept. of Land and Water Resources Engineering, Stockholm, Sweden, 2009.
[54] N. Kuyucak, B. Volesky, Biosorbents for metal recovery of metals from industrial solutions, Biotechnol. Lett. 10 (1988) 137–142.
[55] F. Llanes, D.H. Ryan, R.H. Marchessault, Magnetic nanostructured composites using alginates of different M/G ratios as polymeric matrix, Int. J. Biol. Macromol. 27 (2000) 35–40.
[56] Z. Aksu, Determination of the equilibrium, kinetic and thermodynamic parameters of the batch biosorption of nickel(II) ions onto *Chlorella vulgaris*, Process Biochem. 38 (2002) 89–99.
[57] N Akhtar, J. Iqbal, M. Iqbal, Removal and recovery of nickel(II) from aqueous solution by loofa sponge-immobilized biomass of *Chlorella sorokiniana*: characterization studies, J. Hazard. Mater. 108 (2004) 85–94.
[58] Z.Z. Xu, W.H. Fan, L.J. Feng, Biosorption of nickel by brown algae *Laminaria japonica* immobilized in calcium alginate, Prog. Environ. Sci. Technol. I (2007) 1122–1126.
[59] A. Ozer, G. Gurbuz, A. Calmli, B.K. Korbahti, Investigation of nickel(II) biosorption on *Enteromorpha prolifera*: optimization using response surface analysis, J. Hazard. Mater. 152 (2008) 778–788.
[60] K. Vijayaraghavan, K. Palanivelu, M. Velan, Treatment of nickel containing electroplating effluents with *Sargassum wightii* biomass, Process Biochem. 41 (2006) 853–859.
[61] S. Basha, Z.V.P. Murthy, B. Jha, Isotherm modeling for biosorption of Cu(II) and Ni(II) from wastewater onto brown seaweed, *Cystoseira indica*, AlChE J. 54 (2008) 3291–3302.
[62] A.E. Ofomaja, E.B. Naidoo, S.J. Modise, Dynamic studies and pseudo-second order modeling of copper(II) biosorption onto pine cone powder, Desalination 251 (2010) 112–122.
[63] O.M.M. Freitas, R.J.E. Martins, C.M. Delerue-Matos, R.A.R. Boaventura, Removal of Cd(II), Zn(II) and Pb(II) from aqueous solutions by brown marine macro algae: kinetic modelling, J. Hazard. Mater. 153 (2008) 493–501.
[64] Y. Marcus, Ion Properties, Marcel Dekker, Inc., New York, NY, 1997.
[65] S. Ayoob, A.K. Gupta, P.B. Bhakat, V.T. Bhat, Investigations on the kinetics and mechanisms of sorptive removal of fluoride from water using alumina cement granules, Chem. Eng. J. 140 (2008) 6–14.